ADVANCED MATERIALS
www.advmat.de

A Universal Approach for Room-Temperature Printing and Coating of 2D Materials

*Sina Abdolhosseinzadeh, Chuanfang (John) Zhang, René Schneider, Mahdieh Shakoorioskooie, Frank Nüesch, and Jakob Heier**

Processing 2D materials into printable or coatable inks for the fabrication of functional devices has proven to be quite difficult. Additives are often used in large concentrations to address the processing challenges, but they drastically degrade the electronic properties of the materials. To remove the additives a high-temperature post-deposition treatment can be used, but this complicates the fabrication process and limits the choice of materials (i.e., no heat-sensitive materials). In this work, by exploiting the unique properties of 2D materials, a universal strategy for the formulation of additive-free inks is developed, in which the roles of the additives are taken over by van der Waals (vdW) interactions. In this new class of inks, which is termed "vdW inks", solvents are dispersed within the interconnected network of 2D materials, minimizing the dispersibility-related limitations on solvent selection. Furthermore, flow behavior of the inks and mechanical properties of the resultant films are mainly controlled by the interflake vdW attractions. The structure of the vdW inks, their rheological properties, and film-formation behavior are discussed in detail. Large-scale production and formulation of the vdW inks for major high-throughput printing and coating methods, as well as their application for room-temperature fabrication of functional films/devices are demonstrated.

1. Introduction

With hundreds of discovered members, and thousands more predicted, the big family of 2D materials exhibits an immense range of physical and chemical properties.[1] Most of these materials can be either synthesized by a solution-based method or exfoliated from a layered crystal in a liquid.[2] In either case, the final product is a suspension of 2D nanosheets in a solvent (or solvent mixture) which can be further processed into a printable or coatable ink. The behavior of these suspensions is often described by the Derjaguin–Landau–Verwey–Overbeek (DLVO) theory,[3] which implies that the concentration of the nanosheets in the suspensions has an upper limit above which the suspension becomes unstable.[4] Nevertheless, high-concentration suspensions (inks) are necessary for the formation of percolated particle networks,[5] and fulfilling the rheological requirements of high-throughput printing and coating methods (e.g., high viscosity). Regardless of their concentration, suspensions are thermodynamically unstable, and particles tend to reduce their surface energy by aggregation.[6] To lower the rate of sedimentation, the surface energy difference between the solvent and the 2D material must be minimized,[3] which limits the choices of the dispersion-media to a few solvents whose solubility envelope may not be suitable for subsequent processing.

In conventional ink formulations, additives such as surfactants, binders, and rheology modifiers are used to address the aforementioned problems and process the 2D material suspensions into printable or coatable inks.[7–10] For instance, large concentrations of polymeric binders (e.g., 70 mg mL^{-1} cellulose acetate butyrate) are needed to increase the viscosity of graphene inks to a level that is suitable for screen printing.[11] Since typical additives adversely affect the electronic properties (e.g.,

S. Abdolhosseinzadeh, C. (J.) Zhang, R. Schneider, F. Nüesch, J. Heier
Laboratory for Functional Polymers
Swiss Federal Laboratories for Materials Science and Technology (Empa)
Dübendorf, Switzerland
E-mail: jakob.heier@empa.ch

The ORCID identification number(s) for the author(s) of this article can be found under https://doi.org/10.1002/adma.202103660.

DOI: 10.1002/adma.202103660

S. Abdolhosseinzadeh, F. Nüesch
Institute of Materials Science and Engineering
Swiss Federal Institute of Technology Lausanne (EPFL)
Lausanne, Switzerland

M. Shakoorioskooie
Laboratory for Concrete and Asphalt
Swiss Federal Laboratories for Materials Science and Technology (Empa)
Dübendorf, Switzerland

M. Shakoorioskooie
Center for X-ray Analytics
Swiss Federal Laboratories for Materials Science and Technology (Empa)
Dübendorf, Switzerland

M. Shakoorioskooie
Institute for Building Materials
Swiss Federal Institute of Technology Zürich (ETHZ)
Zürich, Switzerland

conductivity) of the deposited materials[12] and reduce their active surface area, it is crucial to remove them at the end of the fabrication process.[13,14] However, removal of the additives requires thermal treatments (typically at 300–400 °C),[15] which often cannot fully recover the electronic properties (especially for semiconducting materials), limit the choice of materials, complicate the fabrication process, and increase the manufacturing costs.[16] Most of the commercially available polymeric or biodegradable substrates such as poly(ethylene terephthalate) (PET), acrylonitrile butadiene styrene (ABS), poly(lactic acid) (PLA), and paper suffer from low glass-transition or decomposition temperature (usually <150 °C).[17,18] Even when the substrates are heat-resistive, their deformation and/or thermal expansion coefficient mismatches with the deposited layers can lead to thermal-stress induced delamination and cracking of the printed or coated films.[19] Similar problems have been observed with localized or selective heating techniques based on intense-pulsed-light, microwave, or laser, which mainly originate from fast release of gaseous decomposition products, thermal shocks, or steep temperature gradients.[20] Furthermore, in multilayer or multi-component devices with heat-sensitive materials (e.g., biomolecules, or perovskites), thermal treatments even at moderate temperatures (e.g., 80 °C for a methylammonium-lead-iodide-based perovskite solar cell[21]) can lead to drastic chemical degradation and loss of functionality. Therefore, development of room-temperature printable 2D materials inks can not only address the aforementioned challenges but also bring up new, and formerly inconceivable possibilities.

2. Results and Discussion

Here we describe additive-free inks that exploit the unique ability of 2D nanosheets to form percolating networks, accommodating a given solvent. In this novel class of inks, the roles of the traditional additives such as stabilizing the dispersion, adjusting the ink's rheological properties, and binding the particles to each other (cohesion) and the film to the substrate (adhesion), are fully taken over by interparticle van der Waals attractions (vdW inks), enabling completely room-temperature processing of 2D materials. To realize such inks, the nanosheets must be brought close enough to each other to establish the vdW interactions (aggregation) and form a space-filled gel. While the particles' volume fraction is the only requirement for the formation of these gels ($\phi > \phi_{gel}$), the initial aggregated dispersion (**Figure 1**a left) is an inhomogeneous mixture of two phases with unstable rheological properties (Figure 1b) that can neither be printed nor coated. To process such a dispersion into a printable or coatable ink with a steady flow behavior (Figure 1b,c), and capable of forming a continuous film (Figure 1a right), it is necessary to carry out a short and gentle shear-treatment (e.g., by three-roll-milling). This shear-treatment ($\dot{\gamma} < 1000\ s^{-1}$) leads to a substantial and irrecoverable

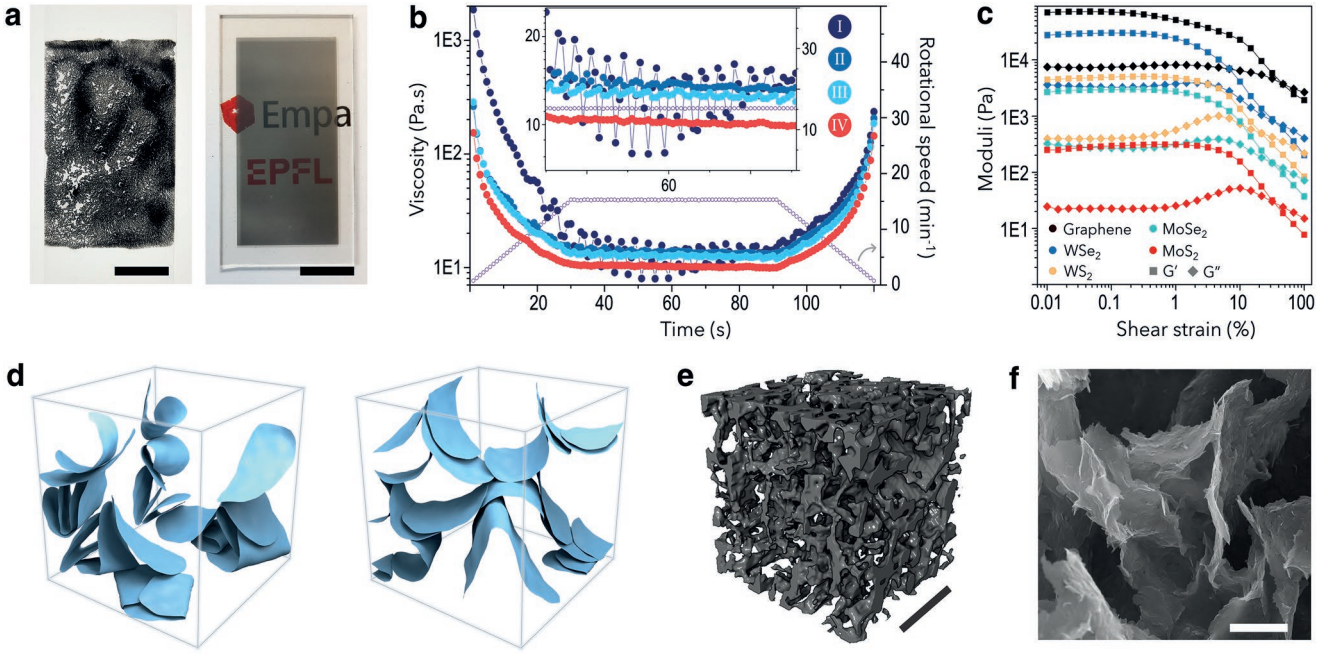

Figure 1. Structure and film-formation of aggregated 2D materials. a) Left: An aggregated graphene dispersion in NMP (1 vol%), capable of forming a gel ($\phi > \phi_{gel}$); Right: A transparent film obtained from the same dispersion after homogenization (low-shear treatment). Scale bars: 1 cm. b) Low-shear treatment of an aggregated dispersion in a dynamic shear rheometer by low-speed rotation of parallel plates. Curve (I): as-obtained aggregated dispersion. The huge irrecoverable drop in the viscosity during the ramp-up stage suggests a structural ordering. Curves (II) and (III): the repetitions of the same test on the same ink with 30 min rest in between. Curve (IV): the same ink after a three-roll-mill treatment. c) Amplitude sweep test of vdW inks made of different 2D materials with different solid contents, confirming their gel structure. d) Schematic illustration of the internal structure of (left) an aggregated dispersion with $\phi > \phi_{gel}$ and (right) the gel obtained after shear-treating the aggregated dispersion. e) Binary X-ray tomogram (scale bar: 40 µm) and f) SEM image (scale bar: 2 µm) of a freeze-dried graphene vdW ink.

drop in the viscosity of the aggregated system (Figure 1b), indicating the flattening and aligning of the crumpled or folded nanosheets (Figure 1d and Video S1, Supporting Information). This results in the formation of a gel (Figure 1c): a homogenous dispersion of a liquid (solvent) within a solid phase (3D network of nanosheets).

The ability of aggregated dispersions to form a film depends on their solid content (volume fraction ϕ of the nanosheets). Upon drying the ink after deposition, the percolated 3D network which incorporates the solvent (Figure 1e,f) collapses, and eventually, a uniform and continuous film is obtained. Lower solid contents correspond to smaller interflake overlapping areas and interaction sites between the aggregated nanosheets (Figure S1, Supporting Information). When the composition of the ink is close to the gel point ($\phi \cong \phi_{gel}$), the 3D network is so weak that even small stresses can lead to the formation of cracks in the wet film (distinct from the typical drying-induced cracking;[22] Figure S1, Supporting Information). At lower concentrations ($\phi < \phi_{gel}$), the 3D network disintegrates into aggregated fractals, and convectional flows of the solvent carry them apart (Figure S1 and Video S1, Supporting Information). In this case, the aggregated dispersion cannot form a continuous film, even though upon drying the volume fraction increases again to above the gel point.

Gelation is a common phenomenon in highly concentrated colloidal systems. However, the structure of the gels and the types of interaction which lead to the gelation differ greatly, ranging from electrostatic and vdW interactions to chemical bonding.[23] In almost all previously reported 2D-material-based gel inks such as graphene-binder,[11] graphene oxide,[24] and MXenes,[25–27] gel formation can be mainly attributed to long-range repulsions between the particles (due to the extended electrical double layers or steric repulsion resulting from the presence of functional groups or adsorbed/grafted surfactant or polymer chains[28]). Therefore, by successive addition of solvent to these types of gels (dilution) a smooth sol–gel transition occurs, and a stable suspension is obtained.[24,25] However, since gel formation in vdW inks is based on the vdW attractions and suspensions of pristine 2D materials are unstable at concentrations close to the gel point, the dilution of gel (below the gel point) leads to a phase separation (Figure S2 and Video S1, Supporting Information). In stark contrast to binder-based gel inks, adding binders to vdW inks actually decreases their yield strength by weakening (interrupting) the interflake vdW attractions (Figure S3, Supporting Information).

A thorough understanding of particle-particle and particle-solvent interactions is necessary for an efficient formulation of inks and adjustment of their properties. Typically, these interactions are indirectly studied by the highest concentration of the 2D material that is dispersible in a specific solvent.[29,30] Similarly, the gel point, defined as "the largest amount of solvent that a 3D network of nanosheets can accommodate", can also be used to evaluate the particle-solvent and particle-particle interactions. In this regard, we prepared several vdW inks in different solvents and measured their gel points. Rheological investigations (comparison of elastic and loss moduli) can be used for the determination of the sol or gel state of the inks. Nevertheless, direct measurement of the gel point, if not impossible, is very difficult, time-consuming, and inaccurate. Gels are very fragile close to their gel points and their formation can sometimes take several hours. To better determine the gel point, we developed an alternative method based on the observation of a power-law relationship between the yield stress of the gels (τ_y) and the volume fraction of the 2D materials ($\tau_y = A\phi^m$, where A and m are constant numbers; **Figure 2**a,b). Conceptually, at the gel point, the strength of the 3D network is just sufficient to overcome the gravitational forces. Hence, it is possible to determine the critical yield stress (τ_{cr}) at which a thin layer of gel collapses under its own weight and estimate the gel point (ϕ_{gel}) by extrapolation of the scaling relation between τ_y and ϕ (Figure 2c).

The critical yield stress (τ_{cr}) for graphene gels was experimentally determined by successive dilution of 4 different inks to their gel points to be between 0.5–1 Pa. Based on this criterion and using the extrapolation method (τ_y versus ϕ), we estimated ϕ_{gel} for 15 different solvents (Figure S4, Supporting Information). To find a relationship between the gel point and the properties of these solvents, ϕ_{gel} was plotted versus their viscosity, surface tension, Hildebrand solubility parameter, Hansen solubility parameter components, and Flory–Huggins parameter (Figure 2d and Figure S5, Supporting Information). Surprisingly, the only clear trend was found when plotting ϕ_{gel} versus viscosity. When increasing the viscosity of the solvents, the gel point decreases, which implies some unexpected conclusions. For instance, the 3D network of graphene nanosheets can accommodate ≈2.3 times (volumetric) more terpineol than *N*-methyl-2-pyrrolidone (NMP), which is a well-known solvent for dispersing graphene. Another example is the equal gel points of the formamide- and quinoline-based inks which are chemically very different but have similar viscosities (Figure S6, Supporting Information).

The yield strength of the gels (and consequently the gel point) also strongly depends on the exfoliation degree of the 2D materials. Gels made with less exfoliated nanosheets (LEG-NMP in Figure 2c) have significantly lower yield strengths for equal volume fractions in a given solvent, which can be attributed to their lower number of interflake interaction sites (vdW attractions). The gel points obtained for other 2D materials (Figure S7, Supporting Information) are higher than in graphene gels; nevertheless, due to the strong dependence of the yield strength on morphological parameters, and considering the large variations in the outcome of the exfoliation processes for different 2D materials (Figures S8 and S9, Supporting Information), drawing a conclusion on the effect of the density of the particles on τ_y is not possible.

The strong dependence of τ_y on morphological factors can be used to evaluate the stability of the inks. Previous theoretical studies[31] suggest that the removal of the last monolayer of solvent from between two graphene sheets (restacking) requires a large energy barrier to be overcome (except for water). No visual signs of restacking were noticed during long-term storage of the inks (>3 months). This was further examined by temporal amplitude sweep tests of a single ink (4 times every 10 days; Figure S10, Supporting Information) where we were unable to observe any change in its yield strength (exfoliation degree). Similar to other colloidal dispersions, phase-separation in the vdW inks is thermodynamically inevitable; however, it is kinetically inhibited especially at higher concentrations ($\phi > 1.1\ \phi_{gel}$)

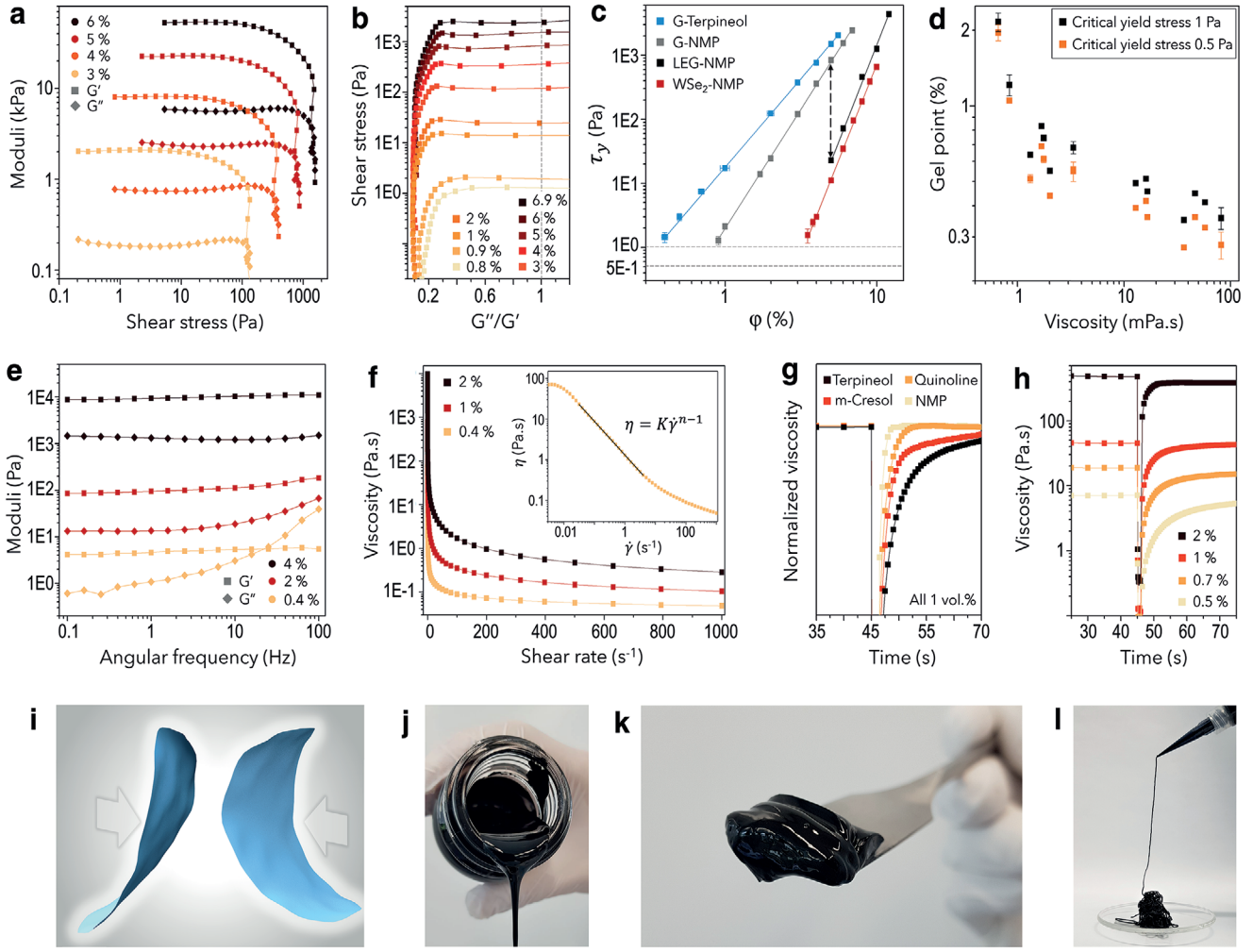

Figure 2. Rheological properties of the vdW inks. a) Amplitude sweep test for 4 different concentrations (vol%) of an NMP–graphene vdW ink. b) Critical yield stress (at $G''/G' = 1$) for successive dilutions (vol%) of an NMP–graphene vdW ink obtained from the amplitude sweep tests. c) The power-law relation between τ_y and ϕ (G: graphene, LEG: less exfoliated graphene). d) Gel points obtained from the intersection of $\tau_y = 1$ Pa and $\tau_y = 0.5$ Pa with extrapolation of the fitted lines in τ_y versus ϕ graphs for graphene gels in 15 solvents with different viscosities. e) Frequency sweep test for 3 concentrations (vol%) of a terpineol–graphene vdW ink. f) Flow curves for 3 concentrations (vol%) of a terpineol–graphene vdW ink (Inset: 0.4 vol% curve plotted in the log–log scale). g) Three-interval thixotropy test (3iTT) of graphene vdW inks with 4 different solvents (viscosities of the solvents: Terpineol = 36.5 mPa s; m-Cresol = 12.9 mPa s; Quinoline = 3.34 mPa s; NMP = 1.68 mPa s). h) 3iTT results of 4 different concentrations (vol%) of a terpineol–graphene vdW ink. i) Schematic illustration of two nanosheets moving toward each other to reaggregate. j–l) Digital photographs of a terpineol–graphene vdW ink at three concentrations for flexographic printing (0.7 vol%) (j), screen printing (2 vol%) (k), and extrusion printing (4 vol%) (l).

and can be neglected in practice (not noticeable even after 6 months). When $\phi \approx \phi_{gel}$, the internal structure of the gel has a small elastic modulus and low cohesive energy density. In such cases, especially under application of excessive external forces (e.g., capillary forces in a tight container), the chance of phase separation is higher. However, even if phase separation occurs, the ink can be easily homogenized by simply stirring it for a few seconds. The long-term stability of the gels was also confirmed by the frequency-independent responses of their elastic and loss moduli at low frequencies in the frequency sweep tests (Figure 2e).

Shear-thinning is an important requirement for printing and coating with high viscosity inks. The viscosity (η) of vdW inks, despite being very high at low shear rates (e.g., >100 Pa.s at rest), drops very fast when increasing the shear rate ($\dot{\gamma}$), and follows the Ostwald–de Waele model ($\eta = K\dot{\gamma}^{n-1}$; Figure 2f and Figure S11, Supporting Information). The power-law index (n) is a measure of shear-thinning behavior and smaller numbers correspond to higher pseudoplasticity.[32] From the double logarithmic plot of η versus $\dot{\gamma}$ (Figure 2f inset), a power-law index $n \approx 0.17$ is obtained which is smaller than for conventional[33] graphene inks ($n \approx 0.4$), suggesting a higher pseudoplasticity. The viscosity of the vdW inks can easily be adjusted over a very wide range (>20 mPa s measured at $\dot{\gamma} = 100\ s^{-1}$) by varying the solvent type and volume fraction of the 2D material, allowing the rheological properties to be adjusted as required for different printing and coating methods (Figure 2f and Figure S11, Supporting Information).

Depending on the printing or the coating method, the as-deposited films may have uneven thickness, discontinuity, or high surface roughness. For instance in screen- or gravure-printing, less or no ink is deposited at certain points because of the mesh or the cell-walls, respectively. After deposition of a pseudoplastic ink, its viscosity, which was decreased upon the application of shear forces, rises back to its initial value as the ink recovers its internal structure. A long enough recovery time allows the height undulations to level out, unconnected segments to merge, or rough surfaces to become smoother. On the other hand, too long recovery times lead to uncontrolled spreading of ink and loss of fidelity. Since various printing or coating techniques require different levels of thixotropic behavior, its optimization is of great importance for ink formulation and high quality printing. Similar to viscosity, the thixotropic behavior of the vdW inks can also be controlled by altering the volume fraction and the solvent type (Figure 2g,h). Nevertheless, it should be noted that inks made with low viscosity solvents show little thixotropy and only at compositions close to their gel point. This limits the application of such inks to deposition techniques that require little or no thixotropy (e.g., an NMP–graphene ink is not suitable for screen-printing but it is a perfect choice for extrusion-printing).

The observed thixotropy is directly related to the viscosity of the solvents, and its likely origin reveals another interesting aspect of the internal structure of the vdW inks. In the absence of polymeric additives and functional groups, the thixotropy can be attributed to the time that is needed for the nanosheets to reaggregate and reconstruct the 3D network which has been broken apart by shearing. The higher the viscosity of the solvent, the longer it takes for the nanosheets to move toward each other, rebuild the gel structure, and enable the ink to regain its initial viscosity (Figure 2g). Lower solid contents correspond to longer travel distances (longer time) and higher thixotropy (Figure 2h). At high volume fractions, the recovery takes place almost instantly and no thixotropy is observed. Considering the aforementioned discussions, the flow behavior of the vdW inks can be easily adjusted over a wide range to fulfill the rheological requirements of common printing and coating methods (Figure 2j–l).

In conventional inks, additives (binders) account for the cohesion of the nanoparticulate film and its adhesion to the substrate. In vdW inks, this role is also taken over solely by the vdW attractions. In fact, in all colloidal gels, vdW attractions are present but their (collective) strength in non-2D materials and less exfoliated 2D materials gels is not sufficient to replace the binders (**Figure 3**a–f and Figure S12, Supporting Information). Owing to their unique morphology, 2D materials can establish the largest amount of vdW interactions between themselves and with the substrate (Figure 3a). Furthermore, compared to other nanomaterials 2D materials can form more efficient interlocks (between nanosheets) and their films can reach higher packing levels (Figure 3b,c). As confirmed by their X-ray diffraction patterns (Figure S13, Supporting Information), after drying, pristine 2D materials can restack and form semicrystalline structures (with substantial amount of vdW interactions), which is not possible in the presence of residual functional groups (Figure 3e). Since the cohesion of the flakes in the parent crystals is lower than in the binder-based films, additive-free films are not expected to exhibit better mechanical properties than their binder-based counterparts. In an abrasive wear test (Figure 3f), under application of a 5 N force

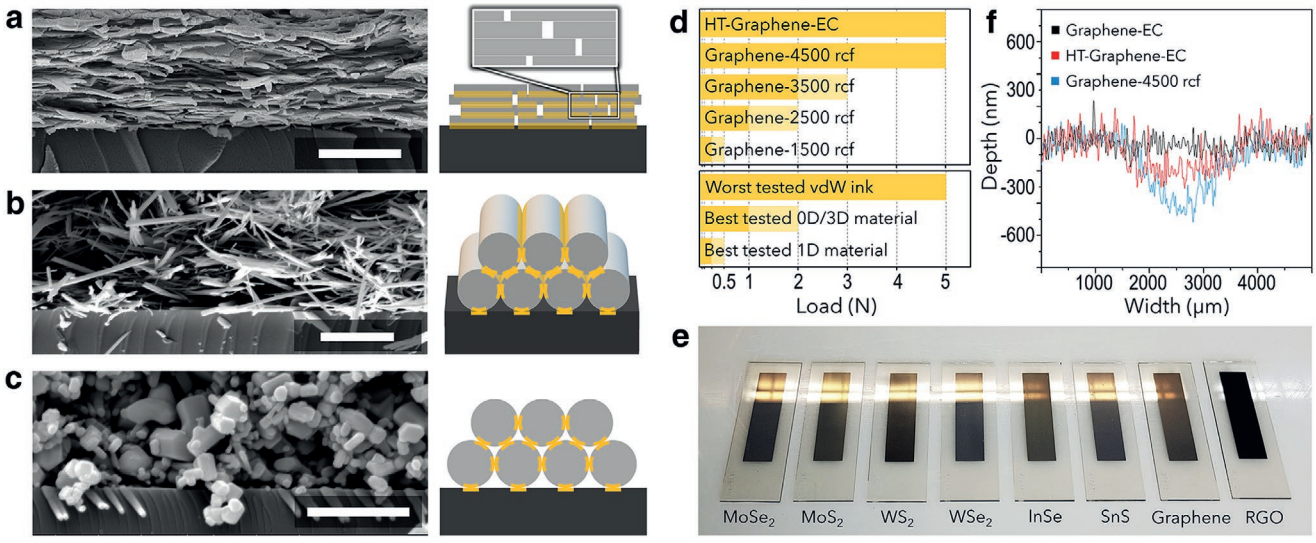

Figure 3. Cohesion and adhesion of additive-free gels. a–c) Cross-sectional SEM images of graphene (scale bar: 1 μm) (a), ZnO nanowires (scale bar: 5 μm) (b), and ZnO nanoparticles (scale bar: 2 μm) (c) films made with additive-free gels. d) Abrasive wear test results. Top: Comparison between adhesion of heat-treated (at 300 °C for 1 h) ethylcellulose-containing graphene ink (HT-graphene-EC) and a graphene vdW ink (Graphene-4500 rcf) to a glass substrate. Inks made with less-exfoliated graphene (centrifuged at 3500, 2500, and 1500 rcf) show significantly lower adhesion. Bottom: Comparison of adhesion (to glass substrates) between vdW inks and gels made with 1D and 0D/3D materials. NMP is used for the formulation of the inks for all of the adhesion test samples. e) Digital image of the films made with different vdW inks. All of the films, after drying, regained a metallic sheen similar to their parent crystals except for reduced graphene oxide (RGO), (width of the glass slide: 2.6 cm). f) Wear test profile for comparison of the particles' cohesion (Graphene-EC: Film obtained from an ethylcellulose-containing ink before heat treatment).

(maximum applicable force by the instrument), ≈400 nm of an additive-free graphene film was removed (≈10% of the film thickness) but the binder-containing film lost only ≈200 nm (≈4%). While the cohesion of 2D nanosheets in the additive-free film is slightly lower than in traditional inks, it is superior to other nanomaterials and is sufficient for most applications.

It should be noted that in applications where the printed structures are exposed to frequent wear and abrasion, applying a protective top layer (e.g., a photocurable polymeric coating, which will not affect the electronic properties) would be necessary (similarly for heat-treated binder-containing films). It is also worth mentioning that, even adding a very small amount of binder (e.g., 0.05–0.1 wt.%; significantly less than the amount that is used in formulation of additive-containing inks[11]) to vdW inks can significantly improve the robustness of the films while having minimal impact on their conductivity. This is due to the fact that the colloidal and rheological properties of the vdW inks, as mentioned earlier can meet the requirements of the printing methods even without the addition of additives, and hence, even very small amounts of binder can be sufficient for formulation of inks with excellent printability and electrical performance. In contrast, in traditional ink formulations, binders play other roles such as adjusting the rheological properties (e.g., increasing viscosity), which require much larger amounts of binders to be added.

Considering the strong dependence of the mechanical properties and adhesion of the additive-free films on the exfoliation level of the 2D materials, it is crucial to use single or few-layered flakes for the preparation of the vdW inks. However, in exfoliation suspensions, which typically contain flakes with different thicknesses and lateral sizes, the few-layered nanosheets have the highest colloidal stability and the lowest concentration.[34] Because of their high stability, separating well-exfoliated nanosheets and increasing their concentration to above gel point is very challenging. Low-pressure evaporation-based methods (e.g., in a rotary evaporator) are extremely energy- and time-consuming since the main exfoliation solvents (e.g., NMP) have high boiling points. High-temperature evaporation can lead to the oxidation/degradation of the solvents[35] or 2D materials.[36] Filtration- and ultrahigh-speed centrifugation-based[5] methods have low yields and can only process small amounts of suspensions. Polymer-assisted extraction techniques[37] are not residual-free and face the same problems as additive-containing inks (for removal of the polymer).

To address the aforementioned challenges and produce vdW inks in large scales (kg), an interface-assisted extraction (IAE) method for controlled aggregation of 2D materials is developed (Figure S14, Supporting Information). For this purpose, after exfoliation of 2D materials and separation of less exfoliated particles (using centrifugation), well-dispersed nanosheets are extracted by forming an emulsion within the exfoliation suspension (see Experimental Section). To reduce the resulting huge interfacial energy, the nanosheets move to the interface of the emulsion microdroplets and cover their surface.[38] Once the phase separation is completed, nanosheets accumulate at the interface of two main phases as a third phase which itself is a metastable Pickering emulsion[39] (**Figure 4**). Due to the density difference and the pressure applied by the other droplets, a part of the solvent leaves the microdroplet, but the rest remains inside the "deflated ball" of 2D nanosheets (Figure 4b–d). Since

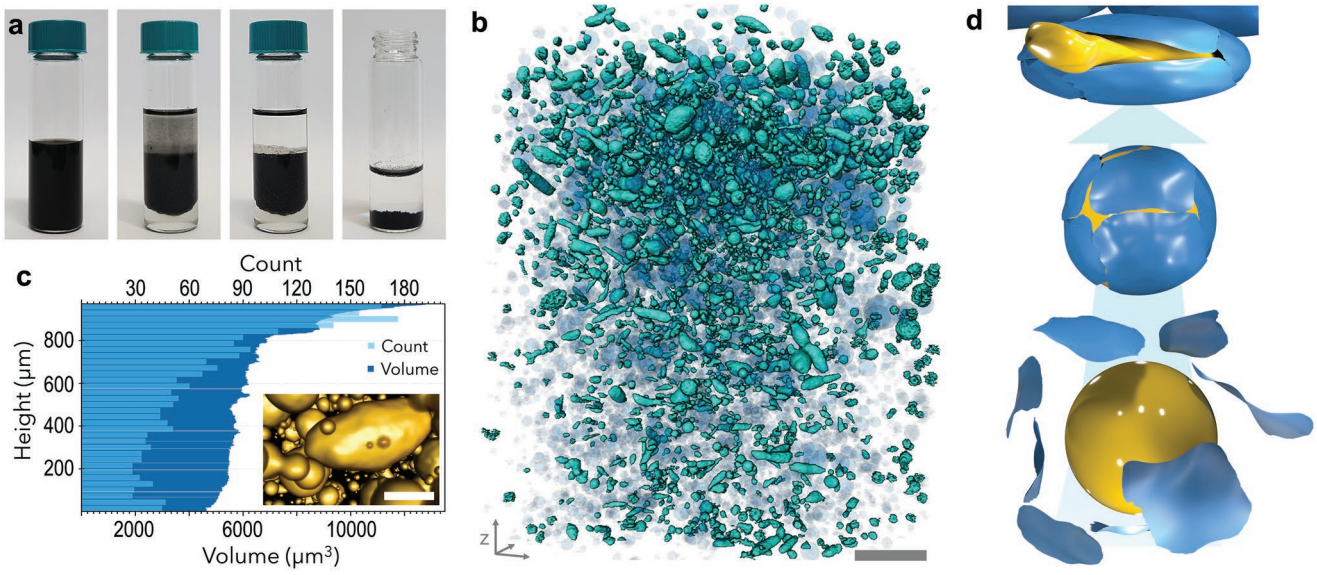

Figure 4. Interface-assisted extraction of 2D materials. a) Formation of a graphene-based Pickering emulsion. From left to right: Toluene is added to a graphene–NMP suspension; water is added to initiate the Pickering emulsion formation and the phase separation; three-phase system remains unchanged even after 4 months; when toluene is allowed to evaporate, graphene nanosheets settle down. b) 3D rendering of the asymmetric microdroplets segmented form the X-ray tomogram of the middle phase in a three-phase system (graphene-based Pickering emulsion made with water–NMP–diiodomethane) formed in a capillary tube. Symmetric microdroplets are shown in blue and semitransparent to increase the visibility of the asymmetric microdroplets (scale bar: 130 μm). c) Count and volume of the asymmetric microdroplets of Pickering emulsion in the middle phase (in the three-phase system shown in (b) increases from one interface toward the other one. Inset: An asymmetric microdroplet in a non-thermodynamically stable state (metastable state; scale bar: 40 μm). d) Schematic illustration of three stages of the deep-metastable-emulsion formation.

the nanosheets on one side are attached to a solvent with lower density, they can remain suspended in the middle phase even under the application of high gravitational forces (12 500 rcf for graphene; Figure S15, Supporting Information). By collecting the highly concentrated middle phase (the Pickering emulsion) and adding a mutual solvent (miscible with both liquid components of the emulsion), aggregated nanosheets precipitate and can be separated, purified, and used for the preparation of vdW inks (see Experimental Section). A mutual solvent (in which all the liquid components of the Pickering emulsion are miscible) is needed for the first step of the purification process; however, the precipitated nanosheets can be later transferred to any other solvent by either successive washing (using centrifugation) in the target solvent, or by evaporation of the mutual solvent (when the target solvent has a higher boiling point).

It is worth mentioning that the highly concentrated precipitates of 2D materials (obtained from the IAE method), in addition to formulating vdW inks, can be used for the production of suspension-type (e.g., an inkjet printing ink) or additive-based inks (e.g., a binder containing screen-printing ink), as such inks also require high concentrations of 2D materials for an efficient printing. When transferred to a low boiling point solvent such as diethyl ether, acetone, ethyl acetate, or ethanol (by washing), the "2D material concentrate" can be easily used for the production of 2D materials based composites (e.g., a graphene-reinforced polymeric composite).

Concentrates of 2D nanosheets can be produced by the IAE method from any stable suspension, regardless of the exfoliation method (e.g., ultrasonic, or high-shear mixing) and/or the utilized solvents (i.e., single solvent (such as NMP) or co-solvent systems (such as water–isopropyl alcohol (IPA))). In the majority of the exfoliation methods, a trade-off should be made between the quality of the nanosheets and their production output; longer exfoliation time leads to higher exfoliation yield but smaller flake size with more defects. While a relatively long exfoliation process has been used in this work (adapted from ref. [40]), it is also possible to shorten the exfoliation time, separate the larger and higher quality nanosheets (at the cost of lower yield) by the IAE method, and repeat the exfoliation process on the unexfoliated particles. This process can be commercially justified since all the solvents that are used for the IAE method can be easily recycled either by phase separation or distillation. It should be also mentioned that other immiscible solvent systems can be used for the IAE method as well, some of which are provided in Table S2, Supporting Information.

To demonstrate the vdW inks' promising potential for room-temperature fabrication of functional devices and films, several inks with different 2D materials and rheological properties were formulated and deposited using common printing and coating methods (**Figure 5**a, Figure S16 and Video S2, Supporting Information). Conductive electrodes and interconnects are indispensable parts of electronic devices and are arguably the most-used components.[41] Flexible and robust graphene films (8% resistivity increase after 18 000 bending cycles, Figure 5b and Figure S17, Supporting Information) with low sheet resistance (as low as ≈3 Ω □$^{-1}$, Figure 5c) were successfully blade-coated on PLA substrates at room-temperature by a terpineol–graphene vdW ink. PLA is a biodegradable polymer and thus of interest for use in disposable electronics and smart packaging.[42] However, it is also one of the most challenging substrates to print conventional 2D materials inks due to its solubility in the well-known exfoliation solvents[43] (e.g., NMP)

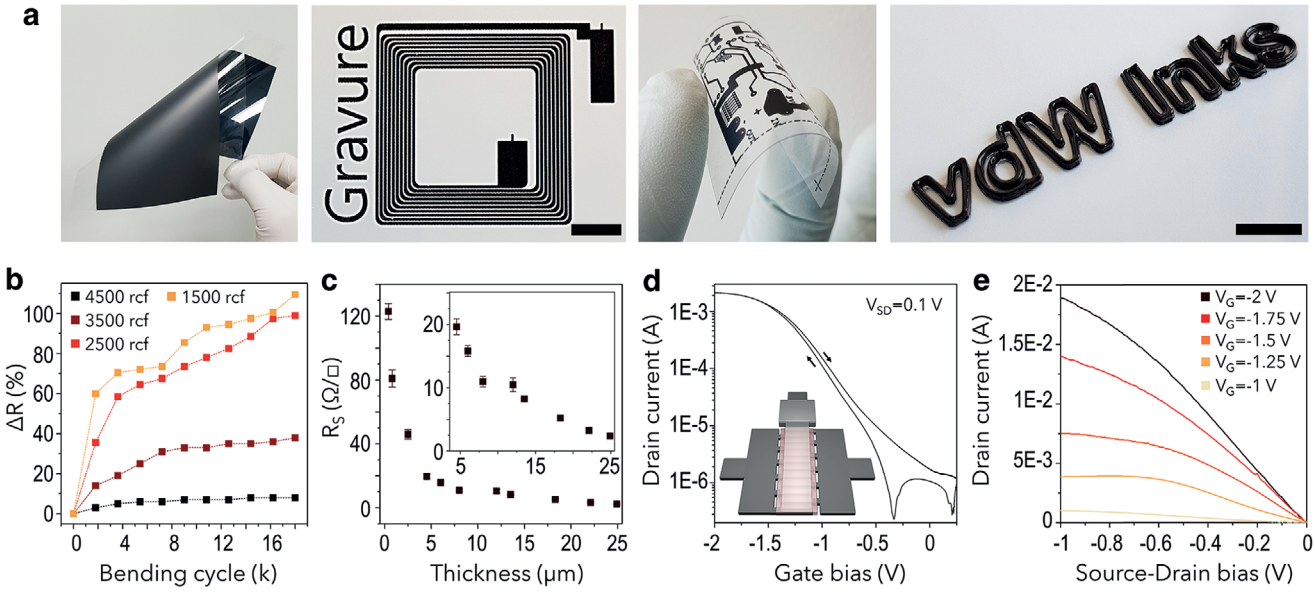

Figure 5. Applications of the vdW inks. a) Left to right: 1) Slot-die coated propylene glycol–graphene vdW ink (0.5 vol%, τ_y = 1.6 Pa) on a PET substrate (size of the substrate: DIN-A5). 2,3) Gravure and flexographic printing of a 0.7 vol% ($\tau_y \cong$ 2 Pa) terpineol–IPA–graphene vdW ink (Terpineol:IPA 80:20) on glossy photo paper and PET substrates (respectively). 4) Extrusion printed 8 vol% NMP–WSe_2 vdW ink on a PET substrate (scale bar: 1 cm). b) Resistance changes of 4 additive-free graphene films with different exfoliation degrees upon 180° bending cycles. c) Sheet resistance of additive-free graphene films (4500 rcf) with different thicknesses (four probe method). d) Transfer and e) output characteristics of a fully printed WSe_2-based electrolyte-gated FET with graphene source/drain/gate electrodes (Inset in (d): schematic representation of the device architecture).

and thermal instability even at low temperatures (T_g = 62 °C for amorphous PLA[44]). It should be noted that while slightly lower resistivity values (e.g., ≈1 Ω □$^{-1}$) have been previously reported for additive-containing inks,[11] they require additional treatments (thermal[45] and/or mechanical[11]) that drastically limit their application. When processed at room-temperature, vdW inks can offer 4–5 orders of magnitude higher conductivity than their additive-based counterparts.[45,46]

The large number of interparticle junctions in particle-based films is the main limiting factor for electric charge transport in nanosheets with high carrier mobility. Therefore, usually relatively thicker films (compared to non-particulate films) are needed to obtain acceptable electrical properties.[5,46] This highlights the importance of high-throughput deposition methods such as screen-printing for the efficient application of particle-based inks (otherwise, multiple overlayer printing, even up to 40 passes will be required[46]). In this work, we also demonstrated the feasibility of screen printing all-2D-material-based field-effect transistors (FET) with vdW inks. Electrolyte gated FETs with a maximum ON/OFF current ratio of ≈2000, a transconductance of 3.13 mS, and a charge carrier mobility of 0.066 cm^2 V^{-1} s^{-1} (Figure 5d,e, Note S1 and Figure S18, Supporting Information), were fully printed at room-temperature on PET substrates with graphene and WSe_2 vdW inks. The majority of previous reports on printed 2D materials-based transistors, are either fabricated with a different device architecture and/or materials combination (e.g., metallic source-drain, or MoS_2 channel), or only have one printed layer (the semiconductor layer is printed and the rest of the layers are either deposited by lithography or spray coating[47–49]), making it difficult to benchmark our results. However, we believe that further improvement of the figures of merit would be possible by optimization of the exfoliation methods or development of new techniques to obtain nanosheets with a larger flake size.[47]

3. Experimental Section

Exfoliation of 2D Materials: Graphite, $MoSe_2$, WSe_2, SnS, and InSe powders were added to NMP, and MoS_2, and WS_2 to 70 vol% water, 30 vol% IPA (all with initial concentrations of 50 mg mL^{-1}), and sonicated for 85 h in a bath sonicator (BANDELIN SONOREX SUPER, 600W, 35kHz). It should be mentioned that the exfoliation method and its parameters (e.g., duration, or the utilized solvents) were not optimized in this work and were chosen according to the literature.[40,34] In principle, vdW inks can be produced from any additive-free suspension of pristine 2D materials; therefore, other liquid-phase exfoliation processes (e.g., different method/power/duration/solvent(s)) can also be used for the production of 2D materials suspensions. A major issue with almost all liquid-phase exfoliation methods was the broad aspect-ratio-distribution of the produced nanosheets, and the low yield of the single-layer flakes (typically <10%).[50,34] However, in most of the applications such as FETs,[51,52] and printed interconnects,[53] multilayer flakes can offer similar or even better performance. Nevertheless, since the aspect-ratio of the nanosheets plays important roles in processing of the vdW inks (e.g., rheological properties of inks and mechanical integrity of the films), it was necessary to separate the less exfoliated nanosheets (discussed in more details within the main text). For this purpose, the obtained suspensions were then centrifuged at 4500 rcf (graphene) or 3500 rcf (MoS_2, $MoSe_2$, WS_2, WSe_2, SnS, and InSe) for 30 min, and the supernatants were collected (Figure S14, Supporting Information). To study the effect of exfoliation degree of the nanosheets, less exfoliated graphene suspensions were obtained by centrifugation at lower speeds (3500 rcf, 2500 rcf, and 1500 rcf). RGO was obtained by a modified Hummers method as described elsewhere.[54]

Preparation of 2D Materials Concentrates via Interface Assisted Extraction (IAE) Method: For NMP-based suspensions (graphene, $MoSe_2$, WSe_2, SnS, and InSe), typically, 500 mL of suspensions and 200 mL xylene were mixed and added to a 1L separation funnel. 300 mL deionized (DI) water was then added to initiate the phase separation (Figure S14, Supporting Information). For MoS_2 and WS_2 suspensions, 300 mL xylene was gradually added to 500 mL of suspension in a separation funnel. In both cases, phase separations and formation of the Pickering emulsions take only a few seconds. The middle phase was separated and washed (3 times) by ethanol (and centrifugation) to obtain the concentrates of each 2D material. The authors have used two different solvent systems (single (NMP) and cosolvent (water–IPA)) to demonstrate that the IAE method can be used for any 2D material suspension and the process was independent of the exfoliation method.

Preparation of vdW Inks: As-obtained concentrates of 2D materials (in ethanol) were further washed 3 times (by centrifugation) with the target solvents (e.g., terpineol for a "terpineol-in-graphene vdW ink"). When the target solvent has a high boiling point, a rotary evaporator can be used to remove the ethanol and transfer the 2D material to the desired solvent. After the last centrifugation step (or alternatively after evaporation of the ethanol), obtained sediments were collected and homogenized with a three-roll-mill (3 passes). To meet the rheological requirements of each printing and coating technique, the solid contents of the inks were adjusted by addition of solvent during the homogenization step. To formulate low viscosity inks (low solid content), which were not processable by a three-roll-mill, the homogenization was carried out at high concentrations (high viscosities), and the composition was adjusted (dilution) by mechanical mixing. An alternative technique, which was suitable for small amounts of inks and/or low viscosity inks has been demonstrated in Video S3, Supporting Information.

Supporting Information

Supporting Information is available from the Wiley Online Library or from the author.

Acknowledgements

The authors gratefully acknowledge financial support from the project FOXIP in the framework of the Strategic Focus Area (SFA) Advanced Manufacturing of the ETH Board, access to the facilities of Empa's Center for X-ray Analytics, the Coating Competence Center (CCC), and the Swiss Scanning Probe Microscopy User Laboratory. The authors would also like to thank Gilberto Siqueira for helping with extrusion printing and Anja Huch for helping with the TEM images.

Open access funding provided by ETH-Bereich Forschungsanstalten.

Conflict of Interest

The authors declare no conflict of interest.

Data Availability Statement

Research data are not shared.

Keywords

additive-free inks, coatings, functional inks, printed electronics, printing, 2D materials

Received: May 14, 2021
Revised: September 29, 2021
Published online: November 30, 2021

[1] N. Mounet, M. Gibertini, P. Schwaller, D. Campi, A. Merkys, A. Marrazzo, T. Sohier, I. E. Castelli, A. Cepellotti, G. Pizzi, N. Marzari, *Nat. Nanotechnol.* **2018**, *13*, 246.
[2] V. Nicolosi, M. Chhowalla, M. G. Kanatzidis, M. S. Strano, J. N. Coleman, *Science* **2013**, *340*, 6139.
[3] Y. Hernandez, M. Lotya, D. Rickard, S. D. Bergin, J. N. Coleman, *Langmuir* **2010**, *26*, 3208.
[4] L. Dong, Z. Chen, X. Zhao, J. Ma, S. Lin, M. Li, Y. Bao, L. Chu, K. Leng, H. Lu, K. P. Loh, *Nat. Commun.* **2018**, *9*, 76.
[5] D. J. Finn, M. Lotya, G. Cunningham, R. J. Smith, D. McCloskey, J. F. Donegan, J. N. Coleman, *J. Mater. Chem. C* **2014**, *2*, 925.
[6] J. N. Coleman, *Acc. Chem. Res.* **2013**, *46*, 14.
[7] T. Carey, S. Cacovich, G. Divitini, J. Ren, A. Mansouri, J. M. Kim, C. Wang, C. Ducati, R. Sordan, F. Torrisi, *Nat. Commun.* **2017**, *8*, 1202.
[8] T. Carey, A. Arbab, L. Anzi, H. Bristow, F. Hui, S. Bohm, G. Wyatt-Moon, A. Flewitt, A. Wadsworth, N. Gasparini, J. M. Kim, M. Lanza, I. McCulloch, R. Sordan, F. Torrisi, *Adv. Electron. Mater.* **2021**, *7*, 2100112.
[9] E. B. Secor, S. Lim, H. Zhang, C. D. Frisbie, L. F. Francis, M. C. Hersam, *Adv. Mater.* **2014**, *26*, 4533.
[10] G. Hu, J. Kang, L. W. T. T. Ng, X. Zhu, R. C. T. T. Howe, C. G. Jones, M. C. Hersam, T. Hasan, *Functional Inks and Printing of Two-Dimensional Materials*, Royal Society Of Chemistry, London, UK **2018**.
[11] K. Pan, Y. Fan, T. Leng, J. Li, Z. Xin, J. Zhang, L. Hao, J. Gallop, K. S. Novoselov, Z. Hu, *Nat. Commun.* **2018**, *9*, 5197.
[12] M. Schneider, E. Koos, N. Willenbacher, *Sci. Rep.* **2016**, *6*, 31367.
[13] E. B. Secor, B. Y. Ahn, T. Z. Gao, J. A. Lewis, M. C. Hersam, *Adv. Mater.* **2015**, *27*, 6683.
[14] S. Abdolhosseinzadeh, J. Heier, C. (J.) Zhang, *J. Phys.: Energy* **2020**, *2*, 031004.
[15] W. J. Hyun, E. B. Secor, M. C. Hersam, C. D. Frisbie, L. F. Francis, *Adv. Mater.* **2015**, *27*, 109.
[16] S. Abdolhosseinzadeh, X. Jiang, H. Zhang, J. Qiu, C. (J.) Zhang, *Mater. Today* **2021**, *48*, 214.
[17] D. Li, W.-Y. Lai, Y.-Z. Zhang, W. Huang, *Adv. Mater.* **2018**, *30*, 1704738.
[18] T. Minari, Y. Kanehara, C. Liu, K. Sakamoto, T. Yasuda, A. Yaguchi, S. Tsukada, K. Kashizaki, M. Kanehara, *Adv. Funct. Mater.* **2014**, *24*, 4886.
[19] D. J. Lee, J. H. Oh, H. S. Bae, *Mater. Lett.* **2010**, *64*, 1069.
[20] Y. R. Jang, S. J. Joo, J. H. Chu, H. J. Uhm, J. W. Park, C. H. Ryu, M. H. Yu, H. S. Kim, *Int. J. Precis. Eng. Manuf. – Green Technol.* **2021**, *8*, 327.
[21] A. Kumar, U. Bansode, S. Ogale, A. Rahman, *Nanotechnology* **2020**, *31*, 365403.
[22] A. F. Routh, *Rep. Prog. Phys.* **2013**, *76*, 046603.
[23] D. H. Everett, *Basic Principles of Colloid Science*, Royal Society of Chemistry, Cambridge, UK **2007**.
[24] S. Naficy, R. Jalili, S. H. Aboutalebi, R. A. Gorkin, K. Konstantinov, P. C. Innis, G. M. Spinks, P. Poulin, G. G. Wallace, *Mater. Horiz.* **2014**, *1*, 326.
[25] B. Akuzum, K. Maleski, B. Anasori, P. Lelyukh, N. J. Alvarez, E. C. Kumbur, Y. Gogotsi, *ACS Nano* **2018**, *12*, 2685.
[26] C. (J.) Zhang, L. McKeon, M. P. Kremer, S. H. Park, O. Ronan, A. Seral-Ascaso, S. Barwich, C. Coileáin, N. McEvoy, H. C. Nerl, B. Anasori, J. N. Coleman, Y. Gogotsi, V. Nicolosi, *Nat. Commun.* **2019**, *10*, 1795.
[27] J. Zhang, S. Uzun, S. Seyedin, P. A. Lynch, B. Akuzum, Z. Wang, S. Qin, M. Alhabeb, C. E. Shuck, W. Lei, E. C. Kumbur, W. Yang, X. Wang, G. Dion, J. M. Razal, Y. Gogotsi, *ACS Cent. Sci.* **2020**, *6*, 254.
[28] T. F. Tadros, *Rheology of Dispersions: Principles and Applications*, Wiley, Hoboken, NJ, USA **2010**.
[29] Y. Hernandez, V. Nicolosi, M. Lotya, F. M. Blighe, Z. Sun, S. De, I. T. McGovern, B. Holland, M. Byrne, Y. K. Gun'ko, J. J. Boland, P. Niraj, G. Duesberg, S. Krishnamurthy, R. Goodhue, J. Hutchison, V. Scardaci, A. C. Ferrari, J. N. Coleman, *Nat. Nanotechnol.* **2008**, *3*, 563.
[30] G. Cunningham, M. Lotya, C. S. Cucinotta, S. Sanvito, S. D. Bergin, R. Menzel, M. S. P. Shaffer, J. N. Coleman, *ACS Nano* **2012**, *6*, 3468.
[31] C. J. Shih, S. Lin, M. S. Strano, D. Blankschtein, *J. Am. Chem. Soc.* **2010**, *132*, 14638.
[32] B. Pang, S. Wang, W. Chen, M. Hassan, H. Lu, *Powder Technol.* **2020**, *366*, 249.
[33] L. W. T. Ng, X. Zhu, G. Hu, N. Macadam, D. Um, T. Wu, F. Le Moal, C. Jones, T. Hasan, *Adv. Funct. Mater.* **2019**, *29*, 1807933.
[34] C. Backes, B. M. Szydłowska, A. Harvey, S. Yuan, V. Vega-Mayoral, B. R. Davies, P. L. Zhao, D. Hanlon, E. J. G. Santos, M. I. Katsnelson, W. J. Blau, C. Gadermaier, J. N. Coleman, *ACS Nano* **2016**, *10*, 1589.
[35] C. Berrueco, P. Álvarez, S. Venditti, T. J. Morgan, A. A. Herod, M. Millan, R. Kandiyoti, *Energy Fuels* **2009**, *23*, 3008.
[36] G. Hu, T. Albrow-Owen, X. Jin, A. Ali, Y. Hu, R. C. T. Howe, K. Shehzad, Z. Yang, X. Zhu, R. I. Woodward, T.-C. Wu, H. Jussila, J.-B. Wu, P. Peng, P.-H. Tan, Z. Sun, E. J. R. Kelleher, M. Zhang, Y. Xu, T. Hasan, *Nat. Commun.* **2017**, *8*, 278.
[37] E. B. Secor, P. L. Prabhumirashi, K. Puntambekar, M. L. Geier, M. C. Hersam, *J. Phys. Chem. Lett.* **2013**, *4*, 1347.
[38] P. Wei, Q. Luo, K. J. Edgehouse, C. M. Hemmingsen, B. J. Rodier, E. B. Pentzer, *ACS Appl. Mater. Interfaces* **2018**, *10*, 21765.
[39] S. Sacanna, W. K. Kegel, A. P. Philipse, *Phys. Rev. Lett.* **2007**, *98*, 158301.
[40] K. R. Paton, E. Varrla, C. Backes, R. J. Smith, U. Khan, A. O'Neill, C. Boland, M. Lotya, O. M. Istrate, P. King, T. Higgins, S. Barwich, P. May, P. Puczkarski, I. Ahmed, M. Moebius, H. Pettersson, E. Long, J. Coelho, S. E. O'Brien, E. K. McGuire, B. M. Sanchez, G. S. Duesberg, N. McEvoy, T. J. Pennycook, C. Downing, A. Crossley, V. Nicolosi, J. N. Coleman, *Nat. Mater.* **2014**, *13*, 624.
[41] J. Perelaer, P. J. Smith, D. Mager, D. Soltman, S. K. Volkman, V. Subramanian, J. G. Korvink, U. S. Schubert, *J. Mater. Chem.* **2010**, *20*, 8446.
[42] N. Halonen, P. S. Pálvölgyi, A. Bassani, C. Fiorentini, R. Nair, G. Spigno, K. Kordas, *Front. Mater.* **2020**, *7*, 82.
[43] S. Sato, D. Gondo, T. Wada, S. Kanehashi, K. Nagai, *J. Appl. Polym. Sci.* **2013**, *129*, 1607.
[44] S. Iannace, L. Nicolais, *J. Appl. Polym. Sci.* **1997**, *64*, 911.
[45] E. B. Secor, T. Z. Gao, A. E. Islam, R. Rao, S. G. Wallace, J. Zhu, K. W. Putz, B. Maruyama, M. C. Hersam, *Chem. Mater.* **2017**, *29*, 2332.
[46] D. McManus, S. Vranic, F. Withers, V. Sanchez-Romaguera, M. Macucci, H. Yang, R. Sorrentino, K. Parvez, S. K. Son, G. Iannaccone, K. Kostarelos, G. Fiori, C. Casiraghi, *Nat. Nanotechnol.* **2017**, *12*, 343.
[47] A. G. Kelly, T. Hallam, C. Backes, A. Harvey, A. S. Esmaeily, I. Godwin, J. Coelho, V. Nicolosi, J. Lauth, A. Kulkarni, S. Kinge, L. D. A. Siebbeles, G. S. Duesberg, J. N. Coleman, *Science* **2017**, *356*, 69.

[48] T. M. Higgins, S. Finn, M. Matthiesen, S. Grieger, K. Synnatschke, M. Brohmann, M. Rother, C. Backes, J. Zaumseil, *Adv. Funct. Mater.* **2019**, *29*, 1804387.
[49] D. O'Suilleabhain, A. G. Kelly, R. Tian, C. Gabbett, D. Horvath, J. N. Coleman, *ACS Appl. Electron. Mater.* **2020**, *2*, 2164.
[50] P. G. Karagiannidis, S. A. Hodge, L. Lombardi, F. Tomarchio, N. Decorde, S. Milana, I. Goykhman, Y. Su, S. V. Mesite, D. N. Johnstone, R. K. Leary, P. A. Midgley, N. M. Pugno, F. Torrisi, A. C. Ferrari, *ACS Nano* **2017**, *11*, 2742.
[51] S. Kim, A. Konar, W. S. Hwang, J. H. Lee, J. Lee, J. Yang, C. Jung, H. Kim, J. B. Yoo, J. Y. Choi, Y. W. Jin, S. Y. Lee, D. Jena, W. Choi, K. Kim, *Nat. Commun.* **2012**, *3*, 1011.
[52] Y. K. Hong, N. Liu, D. Yin, S. Hong, D. H. Kim, S. Kim, W. Choi, Y. Yoon, *J. Phys. D: Appl. Phys.* **2017**, *50*, 164001.
[53] S. Abdolhosseinzadeh, R. Schneider, A. Verma, J. Heier, F. Nüesch, C. Zhang, *Adv. Mater.* **2020**, *32*, 2000716.
[54] S. Abdolhosseinzadeh, H. Asgharzadeh, H. S. Kim, *Sci. Rep.* **2015**, *5*, 10160.